Local multigrid on adaptively refined meshes and multilevel preconditioning with applications to problems in electromagnetism and acoustics

Ronald H. W. Hoppe, Xuejun Xu, Huangxin Chen

Angaben zur Veröffentlichung / Publication details:

Hoppe, Ronald H. W., Xuejun Xu, and Huangxin Chen. 2010. "Local multigrid on adaptively refined meshes and multilevel preconditioning with applications to problems in electromagnetism and acoustics." Augsburg: Universität Augsburg.

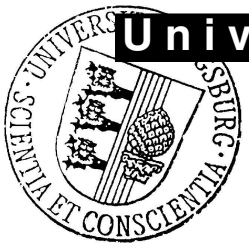

Universität Augsburg

Institut für Mathematik

Ronald H.W. Hoppe, Xuejun Xu, Huangxin Chen

Local Multigrid on Adaptively Refined Meshes and Multilevel Preconditioning with Applications to Problems in Electromagnetism and Acoustics

Preprint Nr. 05/2010 — 26. April 2010

Institut für Mathematik, Universitätsstraße, D-86135 Augsburg http://www.math.uni-augsburg.de/

Impressum:

Herausgeber:

Institut für Mathematik
Universität Augsburg
86135 Augsburg
`http://www.math.uni-augsburg.de/pages/de/forschung/preprints.shtml`

ViSdP:

Ronald H.W. Hoppe
Institut für Mathematik
Universität Augsburg
86135 Augsburg

LOCAL MULTIGRID ON ADAPTIVELY REFINED MESHES AND MULTILEVEL PRECONDITIONING WITH APPLICATIONS TO PROBLEMS IN ELECTROMAGNETISM AND ACOUSTICS

R.H.W. HOPPE*, X. XU†, AND H. CHEN‡

Abstract. We consider local multigrid methods for adaptive finite element and adaptive edge element discretized boundary value problems as well as multilevel preconditioned iterative solvers for the finite element discretization of a special class of saddle point problems. The local multigrid methods feature local smoothing processes on adaptively refined meshes and are applied to adaptive $P1$ conforming finite element discretizations of linear second order elliptic boundary value problems and to adaptive curl-conforming edge element approximations of H(curl)-elliptic problems and the time-harmonic Maxwell equations. On the other hand, the multilevel preconditioned iterative schemes feature block-diagonal or upper block-triangular preconditioned GMRES or BiCGStab applied to the resulting algebraic saddle point problems and preconditioned CG applied to the associated Schur complement system.
As technologically relevant applications of the above methods, we consider the numerical simulation of Logging-While-Drilling tools in oil exploration and the numerical simulation of piezoelectrically actuated surface acoustic waves.

Key words. local multigrid methods, adaptively refined meshes, multilevel preconditioners, saddle point problems, Logging-While-Drilling, surface acoustic waves

AMS subject classifications. 65N30, 65N50, 65N55, 78M10

1. Introduction.

Multigrid or multilevel and domain decomposition methods are the methods of choice when it comes to the efficient numerical solution of large linear systems arising from the finite element discretization of partial differential equations (cf., e.g., [17, 35, 50, 51, 55, 57, 58] and the references therein). For conforming finite elements on quasi-uniform meshes, the convergence properties of multigrid and multilevel methods have been further studied in [16, 18, 21, 67, 68, 69]. A unified framework for a convergence analysis of multilevel and domain decomposition methods has been provided in [64] based on the notions of space decomposition and subspace correction.
On the other hand, during the past three decades adaptive finite element methods based on reliable and/or efficient a posteriori error estimators for local grid adaptation have been intensively studied and have reached some state of maturity as documented by a series of monographs (cf., e.g., [2, 13, 29, 49, 59]). For conforming adaptive finite element discretizations of linear second order elliptic boundary value problems, an overview on convergence results has been given in [47] and optimality has been addressed in [15, 25, 56]. The related issues for adaptive edge element discretizations of H(curl)-elliptic problems and the time-harmonic Maxwell equations have been studied in [24, 38, 71, 72].
Since adaptive grid refinement techniques provide a hierarchy of meshes, it is natural

*Department of Mathematics, University of Houston, Houston, TX 77204-3008, USA, *rohop@math.uh.edu*, and Institute of Mathematics, University at Augsburg, D-86159 Augsburg, Germany, *hoppe@math.uni-augsburg.de*. The work has been supported by the NSF under Grant No. DMS-0810176.

†LSEC, Institute of Computational Mathematics, Chinese Academy of Sciences, P.O.Box 2719, Beijing, 100080, People's Republic of China, *xxj@lsec.cc.ac.cn*. The work of the second and third author has been supported by by the National Basic Research Program of China (Grant No. 2005CB321701) and the National Natural Science Foundation of China (Grant No. 10731060)

‡LSEC, Institute of Computational Mathematics, Chinese Academy of Sciences, P.O.Box 2719, Beijing, 100080, People's Republic of China, *chx@lsec.cc.ac.cn*.

to consider the application of multilevel techniques for adaptively generated meshes which actually has been initiated roughly twenty years ago. The approach in [43, 63] is the fast adaptive composite grid (FAC) method which uses global and local uniform grids both to define the composite grid problem and to interact for achieving a fast solution. Other approaches are the multilevel adaptive technique (MLAT) studied, e.g., in [11, 19] and multigrid methods for locally refined finite element meshes [1, 3, 4, 27, 52]. However, these locally refined meshes are subject to restrictive assumptions which are not met by the newest vertex bisection algorithm which is often used for refinement in the adaptive cycle consisting of the basic steps 'SOLVE', 'ESTIMATE', 'MARK', and 'REFINE'. The paper [62] was the first one to establish convergence of the multigrid V-cycle for nodal based finite element discretizations of linear second order elliptic problems without these restrictions and thus including the newest vertex bisection refinement strategy. The method features a local Gauss-Seidel smoother, i.e., a Gauss-Seidel iteration acting only on new nodes and those old nodes where the support of the associated nodal basis function has changed. Recently, optimality of such local multigrid methods has been shown in [66] based on the Schwarz theory well-known from the domain decomposition methodology [57].

This paper is organized as follows: In section 2, we will be concerned with local multigrid methods for adaptive finite element discretizations of linear second order elliptic boundary value problems and adaptive edge element discretizations of boundary value problems for H(curl)-elliptic equations and the time-harmonic Maxwell equations. Level-independent multigrid convergence rates are derived within the Schwarz theory under assumptions that have to verified for the local smoothers involved in the local multigrid methods. Section 3 is devoted to multilevel preconditioned iterative schemes for a special class of saddle point problems featuring block preconditioned GMRES and BiCGStab as well as preconditioned CG for the associated Schur complement system. The final sections 4 and 5 deal with technologically relevant applications. In particular, in section 4 we consider the numerical simulation of Logging-While-Drilling (LWD) tools that are used in oil exploration for measuring relevant geohydraulic parameters of the geological formation surrounding a borehole during the drilling process. For LWD tools with electromagnetic transmitters and receivers, the forward problem amounts to the solution of the time-harmonic Maxwell equations which can be solved using those local multigrid methods described in section 2. In section 5, we study the numerical solution of piezoelectrically actuated surface acoustic waves (SAW). SAW can be used, e.g., for signal processing in telecommunications or as nano-pumps in a microfluidic lab-on-a-chip. Such chips have their applications in clinical diagnostics, pharmacology, and forensics for high-throughput screening and hybridization in genomics, protein profiling in proteomics, and cytometry in cell analysis. The mathematical model gives rise to a saddle point problem of the form studied in section 3 and can thus be numerically solved by multilevel preconditioned iterative solvers.

2. Local Multigrid Methods on Adaptively Generated Meshes. In this section and throughout the rest of the paper, we use standard notation from Lebesgue and Sobolev space theory. In particular, for a bounded domain $\Omega \subset \mathbb{R}^d, d \in \mathbb{N}$, we denote by $L^2(\Omega)$ and $\mathbf{L^2}(\Omega) := L^2(\Omega)^d$ the Hilbert spaces of square-integrable scalar- and vector-valued functions on Ω, respectively. Further, we denote by $H^1(\Omega)$ the Sobolev space of square integrable functions with square integrable weak derivatives equipped with the inner product $(\cdot,\cdot)_{1,\omega}$ and norm $\|\cdot\|_{1,\Omega}$. For $\Sigma \subseteq \partial\Omega$, we refer to $H^{1/2}(\Sigma)$ as the space of traces $v|_\Sigma$ of functions $v \in H^1(\Omega)$ on Σ. We set $H^1_{0,\Sigma}(\Omega) :=$

$\{v \in H^1(\Omega) | v|_\Sigma = 0\}$ and refer to $H_\Sigma^{-1}(\Omega)$ as the associated dual space. For a simply connected polyhedral domain Ω with boundary $\Gamma = \partial\Omega$ we refer to $\mathbf{H}(\mathbf{curl};\Omega)$ as the Hilbert space of vector fields $\mathbf{q} \in \mathbf{L^2}(\Omega)$ such that $\boldsymbol{\nabla}\times\mathbf{q} \in \mathbf{L^2}(\Omega)$, equipped with the standard graph norm $\|\cdot\|_{curl,\Omega}$. We denote by $\mathbf{H_0}(\mathbf{curl};\Omega)$ the subspace of vector fields with vanishing tangential trace components on Γ.

We assume V and H to be Hilbert spaces of functions on Ω with inner products $(\cdot,\cdot)_V, (\cdot,\cdot)_H$ and associated norms $\|\cdot\|_V, \|\cdot\|_H$ such that $V \subset H \subset V^*$ and V is continuously embedded in H. Given a bounded, V-elliptic bilinear form $a(\cdot,\cdot) : V \times V \to \mathbb{R}$ and a bounded linear functional $\ell \in V^*$, we consider the variational equation: Find $u \in V$ such that

$$a(u,v) \;=\; \ell(v) \quad , \quad v \in V. \tag{2.1}$$

In view of the Lemma of Lax-Milgram [26], the variational equation (2.1) admits a unique solution $u \in V$.

Example 1: A typical example is $V = H_0^1(\Omega), H = L^2(\Omega)$ and

$$a(u,v) \;=\; \int_\Omega \Big(a\nabla u \cdot \nabla v + cuv \Big)\, d\mathbf{x} \quad , \quad \ell(v) := \int_\Omega fv \; d\mathbf{x}, \tag{2.2}$$

where $f \in L^2(\Omega)$, $a = (a_{ij})_{i,j=1}^d, a_{ij} \in L^\infty(\Omega), 1 \le i,j \le d$, is a symmetric, uniformly positive definite matrix-valued function, and $c \in L_+^\infty(\Omega)$. Here, (2.1) represents the weak formulation of a second order elliptic boundary value problem.

Example 2: Another example is $V = \mathbf{H_0}(\mathbf{curl};\Omega), H = \mathbf{L^2}(\Omega)$ with

$$a(u,v) \;=\; \int_\Omega \Big(a(\nabla\times u)\cdot(\nabla\times v) + cu\cdot v \Big)\, d\mathbf{x} \quad , \quad \ell(v) := \int_\Omega f\cdot v \; d\mathbf{x}, \tag{2.3}$$

where $f \in \mathbf{L^2}(\Omega)$, $a \in L^\infty(\Omega)$ such that $a(x) \ge a_0 > 0$ a.e. in Ω, and $c \in L^\infty(\Omega)$. In case $c \in L_+^\infty(\Omega)$, the variational equation (2.1) is the weak formulation of an H(curl)-elliptic boundary value problem, e.g., arising from a semi-discretization in time of the eddy currents equations. On the other hand, if $c(x) < 0$ a.e. in Ω as it is the case for the Helmholtz problem associated with the time-harmonic Maxwell equations, the bilinear form $a(\cdot,\cdot)$ is not V-elliptic, but satisfies a Gårding-type inequality. Under suitable assumptions on the data it can be shown that for the solution of (2.1) a Fredholm alternative holds true (cf., e.g., [45]).

We assume $(V_i)_{i=0}^L, L \in \mathbb{N}$, $V_i = \mathrm{span}\{\varphi_1^{(i)}, \cdots, \varphi_{N_i}^{(i)}\}, N_i \in \mathbb{N}, 0 \le i \le L$, to be a nested sequence $V_{i-1} \subset V_i, 1 \le i \le L$, of finite dimensional subspaces of V obtained, e.g., with respect to a nested hierarchy $\mathcal{T}_i(\Omega)$ of simplicial triangulations of Ω generated by the application of adaptive finite element methods to (2.1). For $D \subset \bar{\Omega}$ we refer to $\mathcal{N}_i(D), \mathcal{E}_i(D)$, and $\mathcal{F}_i(D)$ as the sets of nodes, edges, and faces of $\mathcal{T}_i(\Omega)$ in D. Moreover, for $E \in \mathcal{E}_i(D), F \in \mathcal{F}_i(D)$, and $T \in \mathcal{T}_i(\Omega)$ we denote by h_E the length of E, and by h_F and h_T the diameters of F and T, respectively. We set $h_i := \max\{h_T \mid T \in \mathcal{T}_i(\Omega)\}$.
The Galerkin approximation of (2.1) with respect to $V_i \subset V, 0 \le i \le L$, reads: Find $u_i \in V_i$ such that

$$a(u_i,v_i) \;=\; \ell(v_i) \quad , \quad v_i \in V_i. \tag{2.4}$$

If we define $A_i : V_i \to V_i$ by $(A_i u, v)_H = a(u, v), u, v \in V_i$, and $b_i \in V_i$ by $(b_i, v)_H = \ell(v), v \in V_i$, then 2.4 can be equivalently written as

$$A_i u_i \;=\; b_i. \tag{2.5}$$

Example 1: For (2.1) with $V = H_0^1(\Omega), H = L^2(\Omega)$ and the bilinear form $a(\cdot,\cdot)$ being given by (2.2), the natural choice for a finite element discretization is to choose nodal based conforming finite elements with respect to the simplicial triangulations $\mathcal{T}_i(\Omega)$ such as the Lagrangean finite elements of type (k) [26]. In particular, for $k = 1$ we obtain

$$V_i := \{v \in C_0(\Omega) \mid v|_T \in P_1(T)\ ,\ T \in \mathcal{T}_h(\Omega)\}, \tag{2.6}$$

where $P_1(T)$ stands for the set of polynomials of degree 1 on T. The basis functions $\varphi_j^{(i)}, 1 \le j \le N_i$, are the nodal basis functions associated with the interior nodes $a_k \in \mathcal{N}_i(\Omega), 1 \le k \le N_i$, such that $\varphi_j^{(i)}(a_k) = \delta_{jk}, 1 \le j, k \le N_i$.
A hierarchy of adaptively refined meshes can be obtained, e.g., by residual-type a posteriori error estimators consisting of element residuals and edge residuals in 2D resp. element and face residuals in 3D (cf., e.g., [59]).

Example 2: In case $V = \mathbf{H_0(curl;\Omega)}, H = \mathbf{L^2}(\Omega)$ and $a(\cdot,\cdot)$ given by (2.3), a convenient choice for a curl-conforming finite element discretization are the edge elements of Nédélec's first family [48]

$$\mathbf{Nd^1}(T) := \{\mathbf{q} \mid \mathbf{q}(\mathbf{x}) = \mathbf{a} + \mathbf{b}\times\mathbf{x}\ ,\ \mathbf{a},\mathbf{b} \in \mathbb{R}^3\}\ ,\ T \in \mathcal{T}_i(\Omega), \tag{2.7}$$

where each $\mathbf{q} \in \mathbf{Nd^1}(T)$ is uniquely determined by the zero moments of its tangential components on the six edges of T. This gives rise to the curl-conforming edge element spaces

$$V_i := \{v \in \mathbf{H_0(curl;\Omega)} \mid v|_T \in \mathbf{Nd^1}(T)\ ,\ T \in \mathcal{T}_i(\Omega)\}. \tag{2.8}$$

The basis functions $\varphi_j^{(i)}, 1 \le j \le N_i$, are the vector-valued functions associated with the interior edges $E_k \in \mathcal{E}_i(\Omega), 1 \le k \le N_i$, such that

$$h_{E_k}^{-1} \int_{E_k} \mathbf{t}_{E_k} \cdot \varphi_j^{(i)}\ ds \;=\; \delta_{jk}\ ,\ 1 \le j, k \le N_i, \tag{2.9}$$

where $\mathbf{t}_{E_k}$ denotes the unit tangential vector on E_k.
Residual-type a posteriori error estimators for these edge element discretizations have been first studied in [14] and subsequently considered in [24, 38, 71, 72].

We will solve (2.5) on level $i = L$ by local multigrid methods. As mentioned in the introductory section 1, local multigrid methods differ from standard multigrid schemes in so far as they feature local instead of global smoothing. To this end, we introduce

$$\mathcal{J}_i := \{1 \le j \le N_i \mid \nexists\ 1 \le j_{i-1} \le N_{i-1} \text{ s.th. } \varphi_i^{(j)} = \varphi_{i-1}^{(j_{i-1})}\} \tag{2.10}$$

as the set of all indices $1 \le j \le N_i$ for which the level i basis function $\varphi_i^{(j)}$ does not correspond to a level $i-1$ basis function. Setting

$$\tilde{N}_i := \mathrm{card}(\mathcal{J}_i), \tag{2.11}$$

we rearrange the set of basis functions $\varphi_i^{(j)}, 1 \leq j \leq N_i$, according to

$$\{\varphi_i^{(1)}, \cdots, \varphi_i^{(\tilde{N}_i)}, \varphi_i^{(\tilde{N}_i+1)}, \cdots, \varphi_i^{(N_i)}\}, \tag{2.12}$$

such that $\varphi_i^{(j)}, 1 \leq j \leq \tilde{N}_i$, are the basis functions associated with the set $\mathcal{J}_i$ given by (2.10). For $1 \leq i \leq L$, we refer to $R_i : V_i \to V_i$ as a local smoothing operator that only operates on $\varphi_i^{(j)}, 1 \leq j \leq \tilde{N}_i$, whereas for $i = 0$ we choose $R_0 = A_0^{-1}$. We define projections $P_i, Q_i : V_L \to V_i, 0 \leq i \leq L-1$, by

$$a(P_i v, w) = a(v, w) \quad , \quad (Q_i v, w)_H = (v, w)_H \quad , \quad v \in V_L \ , \ w \in V_i. \tag{2.13}$$

Setting $V_i^{(j)} := \text{span}\{\varphi_i^{(j)}\}, 1 \leq j \leq N_i$, we further define local projections $P_i^{(j)}, Q_i^{(j)} : V_L \to V_i^{(j)}$ and $A_i^{(j)} : V_i^{(j)} \to V_i^{(j)}$ according to

$$a(P_i^{(j)} v, \varphi_i^{(j)}) = a(v, \varphi_i^{(j)}) \quad , \quad (Q_i^{(j)} v, \varphi_i^{(j)})_H = (v, \varphi_i^{(j)})_H \quad , \quad v \in V_L, \tag{2.14}$$

$$(A_i^{(j)} v, \varphi_i^{(j)})_H = a(v, \varphi_i^{(j)}) \quad , \quad v \in V_i^{(j)}. \tag{2.15}$$

Then, the **local multigrid V-cycle** solves (2.5) by the iterative scheme

$$u_i^{(n+1)} = u_i^{(n)} + B_i(b_i - A_i u_i^{(n)}) \quad , \quad 0 \leq i \leq L \ , \ n \in \mathbb{N}_0. \tag{2.16}$$

Here, the operators $B_i, 0 \leq i \leq L$, are recursively given by $B_0 := A_0^{-1}$, whereas for $i \geq 1$ and $c \in V_i$ we define $B_i c = z_3$ with z_3 obtained by pre-smoothing, coarse-grid correction. and post-smoothing according to

Pre-smoothing: $z_1 = R_i b_i$,
Correction: $z_2 = z_1 + B_{i-1} Q_{i-1}(c - A_i z_1)$,
Post-smoothing: $z_3 = z_2 + R_i(c - A_i z_2)$.

Example 1: We consider the local Jacobi and the local Gauss-Seidel smoother. The local Jacobi smoother is an additive smoother given by

$$R_i := \gamma \sum_{j=1}^{\tilde{N}_i} (A_i^{(j)})^{-1} Q_i^{(j)}, \tag{2.17}$$

where $\gamma > 0$ is an appropriately chosen scaling parameter. On the other hand, the local Gauss-Seidel smoother is a multiplicative smoother given by

$$R_i := (I - E_i) A_i^{-1} \quad , \quad E_i := \prod_{j=1}^{\tilde{N}_i} (I - P_i^{(j)}). \tag{2.18}$$

Example 2: It is well known that for H(curl)-elliptic problems and the time-harmonic Maxwell equations the smoothing process has to take into account the non-trivial kernel of the discrete curl-operator which is given by the gradients of the nodal basis functions spanning the P_1-conforming finite element space (cf., e.g., [45]). In fact, one has to use a hybrid smoother which smoothes with respect to both the edge basis functions and the gradients of the nodal basis functions. Appropriate hybrid smoothers are the Hiptmair smoother [36, 37] and the Arnold-Falk-Winther smoother [7]. For local multigrid, the local version of the Hiptmair-Jacobi smoother

is given as follows: We assume $N_i = \mathrm{card}(\mathcal{E}_i(\Omega)), M_i = \mathrm{card}(\mathcal{N}_i(\Omega))$ and refer to $\psi_i^{(j)}, 1 \le j \le N_i$, and $\theta_i^{(j)}, 1 \le j \le M_i$, as the edge and nodal basis functions, respectively. We define $\tilde{N}_i, \tilde{M}_i$ as in (2.10),(2.11) and set

$$\varphi_i^{(j)} := \begin{cases} \psi_i^{(j)} \ , \ 1 \le j \le \tilde{N}_i \\ \nabla\theta_i^{(j-\tilde{N}_i)} \ , \ \tilde{N}_i + 1 \le j \le \tilde{N}_i + \tilde{M}_i \end{cases} . \tag{2.19}$$

Then, the local Hiptmair-Jacobi smoother is the additive smoother given by

$$R_i := \gamma \sum_{j=1}^{\tilde{N}_i+\tilde{M}_i} (A_i^{(j)})^{-1} Q_i^{(j)}, \tag{2.20}$$

where $\gamma > 0$ is a scaling factor. The multiplicative Hiptmair-Gauss-Seidel smoother can be defined analogously.

The optimality of the local multigrid method in terms of level-independent convergence rates can be shown based on the well-known Schwarz theory as described, e.g., in [57, 64, 69]. For this purpose, we define operators $T : V_L \to V_L$ and $T_i : V_L \to V_i, 0 \le i \le L$, according to

$$T := \sum_{i=0}^{L} T_i \quad , \quad T_i := R_i A_i P_i \ , \ 0 \le i \le L. \tag{2.21}$$

The convergence of the local multigrid method will be measured in terms of the error operator

$$E := \prod_{i=0}^{L} (I - T_i), \tag{2.22}$$

where I stands for the identity in V_L.

THEOREM 2.1. *We suppose that the operators $T_i, 0 \le i \le L$, and T satisfy the following assumptions:*

($\mathbf{A_1}$)*: The operators $T_i, 0 \le i \le L$, are nonnegative with respect to the inner product $a(\cdot,\cdot)$, and there exist constants $0 < \omega_i < 2, 0 \le i \le L$, such that for all $v \in V_L$*

$$a(T_i v, T_i v) \ \le \ \omega_i \ a(T_i v, v) \quad , \quad 0 \le i \le L. \tag{2.23}$$

($\mathbf{A_2}$)*: There exists a stability constant $C_0 > 0$ such that for all $v \in V_L$*

$$a(v, v) \ \le \ C_0 \ a(Tv, v). \tag{2.24}$$

($\mathbf{A_3}$)*: There exist constants $C_\nu > 0, 1 \le \nu \le 2$, such that for all $v, w \in V_L$*

$$\sum_{i=0}^{L} \sum_{j=0}^{i-1} a(T_i v, T_j w) \ \le \ C_1 \ \Big(\sum_{i=0}^{L} a(T_i v, v) \Big)^{1/2} \ \Big(\sum_{i=0}^{L} a(T_i w, w) \Big)^{1/2}, \tag{2.25a}$$

$$\sum_{i=0}^{L} a(T_i v, w) \ \le \ C_2 \ \Big(\sum_{i=0}^{L} a(T_i v, v) \Big)^{1/2} \ \Big(\sum_{i=0}^{L} a(T_i w, w) \Big)^{1/2}. \tag{2.25b}$$

Under these assumptions, the local multigrid method converges with

$$a(Ev, Ev) \;\leq\; \gamma\; a(v, v) \quad , \quad v \in V_L, \tag{2.26}$$

where $\gamma := 1 - (2-\omega)/(C_0(C_1+C_2)^2), \omega := \max_{0\leq i\leq L} \omega_i$.

Proof. We refer to [57, 64] or [69]. □

In order to apply Theorem 2.1 to the local multigrid methods from Example 1 and Example 2 above, one has to verify the assumptions ($\mathbf{A_1}$),($\mathbf{A_2}$), and ($\mathbf{A_3}$) for the respective local smoothers. As far as the local Jacobi and local Gauss-Seidel smoothers from Example 1 are concerned, this has been done in [66]. For the local Hiptmair-Jacobi and local Hiptmair-Gauss-Seidel smoothers from Example 2, similar arguments can be applied.

3. Multilevel Preconditioning of Saddle Point Problems. We assume V,H, and W to be Hilbert spaces of real- or complex-valued functions with inner products $(\cdot,\cdot)_V, (\cdot,\cdot)_H, (\cdot,\cdot)_W$ and associated norms $\|\cdot\|_V, \|\cdot\|_Q, \|\cdot\|_W$ such that $V \subset H \subset V^*$ and V is compactly embedded in H. We further suppose that $a(\cdot,\cdot) : V \times V \to \mathbb{K}$, $\mathbb{K} = \mathbb{R}$ or $\mathbb{K} = \mathbb{C}$, is a bounded, symmetric (resp. Hermitean) and V-elliptic bilinear (resp. sesquilinear) form, $b(\cdot,\cdot) : W \times V \to \mathbb{K}$ is a bounded bilinear (resp. sesquilinear) form, and $c(\cdot,\cdot) : W \times W \to \mathbb{K}$ is a bounded, symmetric (resp. Hermitean) and W-elliptic bilinear (resp. sesquilinear) form. We set $a_\omega(\cdot,\cdot) := a(\cdot,\cdot) - \omega^2(\cdot,\cdot)_H$, where $\omega \in \mathbb{R}_+$. Given bounded linear functionals $\ell_1 : V \to \mathbb{K}$ and $\ell_2 : W \to \mathbb{K}$, we consider saddle point problems of the form: Find $(u, w) \in V \times W$ such that

$$a_\omega(u, v) + b(w, v) = \ell_1(v) \quad , \quad v \in V, \tag{3.1a}$$
$$b(u, z) - c(w, z) \quad = \ell_2(z) \quad , \quad z \in W. \tag{3.1b}$$

In case $\omega = 0$ and $\mathbb{K} = \mathbb{R}$, such problems arise, e.g., from the mixed formulation of elliptic boundary value problems and the weak formulation of the Stokes problem, where typically $c(\cdot,\cdot) = 0$ (cf., e.g., [22]), whereas for $\omega > 0$ they occur within the context of time-harmonic acoustics or time-harmonic electromagnetism ($\mathbb{K} = \mathbb{C}$) (cf., e.g., [45]). In section 5, we will deal with a problem representing the weak formulation of a model for piezoelectrically actuated surface acoustic waves.

We denote by $A : V \to V^*, B : W \to V^*$, and $C : W \to W^*$ the operators associated with the bilinear (sesquilinear) forms and by I the injection $I : V \to V^*$. Then, an equivalent formulation of (3.1a),(3.1b) is

$$(A - \omega^2\, \mathbf{I})u \;+\; Bw \;=\; \ell_1 \;, \tag{3.2a}$$
$$B^*u \;-\; Cw \qquad\quad = \;\ell_2 \;, \tag{3.2b}$$

where $B^* : V \to W^*$ stands for the adjoint of B. In particular, the operator A is self-adjoint and V-elliptic, and the operator C is self-adjoint and W-elliptic. In the sequel, we focus on the case where the operator C is invertible. Then, an elimination of w from (3.2a),(3.2b) results in the Schur complement system

$$(S - \omega^2 I)u \;=\; \ell. \tag{3.3}$$

Here, the operator $S : V \to V^*$ is defined according to

$$S \;:=\; A \;+\; BC^{-1}B^*, \tag{3.4}$$

whereas the right-hand side ℓ is given by

$$\ell \;:=\; \ell_1 \;+\; BC^{-1}\ell_2. \tag{3.5}$$

THEOREM 3.1. *If $S^{-1} : Q \to V$ is a Hilbert-Schmidt operator, there holds:*

(i) The spectrum of S consists of a sequence of countably many real eigenvalues $0 < \zeta_1^2 < \zeta_2^2 < \dots$ tending to infinity, i.e., $\lim_{j\to\infty} \zeta_j^2 = \infty$.

(ii) If ω^2 is not an eigenvalue of S, for every $\ell \in V^*$, (3.3) admits a unique solution $u \in V$ depending continuously on ℓ.

(iii) If ω^2 is an eigenvalue of S, (3.3) is solvable if and only if $\ell \in Ker(S-\omega^2 I)^0$ where

$$Ker(S-\omega^2 I)^0 \;:=\; \{v^* \in V^* \mid \langle v^*, v\rangle = 0 \ ,\ v \in Ker(S-\omega^2 I)\}.$$

Proof. The assertions $(i), (ii)$, and (ii) follow from the Hilbert-Schmidt theory and the Fredholm alternative (cf., e.g., [70]). □

COROLLARY 3.2. *If $\omega \in \mathbb{R}$ is such that (3.3) is solvable, then the operator $S_\omega := S - \omega^2 I$ satisfies the inf-sup condition*

$$\inf_{0\neq u\in V} \sup_{0\neq v\in V} \frac{|\langle \mathbf{S}_\omega u, v\rangle|}{\|u\|_V \|v\|_V} \;\geq \beta > 0. \tag{3.6}$$

Proof. We refer to [22]. □

Given a null sequence $\mathcal{H}$ of positive real numbers, we assume $(V_h)_{h\in\mathcal{H}}, V_h \subset V, h \in \mathcal{H}$, and $(W_h)_{h\in}, W_h \subset W, h \in \mathcal{H}$, to be sequences of finite dimensional subspaces that are limit dense in V and W, respectively. The Galerkin approximation of the saddle point problem (3.1a),(3.1b) amounts to the computation of $(u_h, w_h) \in V_h \times W_h$ such that

$$a_\omega(u_h, v_h) \;+\; b(w_h, v_h) \;= \ell_1(v_h) \quad , \quad v_h \in V_h, \tag{3.7a}$$
$$b(z_h, u_h) \;-\; c(w_h, z_h) \quad = \ell_2(z_h) \quad , \quad w_h \in W_h. \tag{3.7b}$$

We denote by $A_h : V_h \to V_h^*, B_h : W_h \to V_h^*, C_h : W_h \to W_h^*$ the operators associated with the restrictions $a|_{V_h\times V_h}, b|_{W_h\times V_h}, c|_{W_h\times W_h}$, and by I_h the injection $I_h : V_h \to V_h^*$, and we further define $\ell_{1,h} \in V_h^*$ and $\ell_{2,h} \in W_h^*$ analogously. Then, the operator form of (3.7a),(3.7b) reads as follows:

$$(A_h - \omega^2 I_h)u_h \;+\; B_h w_h = \ell_{1,h} \ , \tag{3.8a}$$
$$B_h^* u_h \;-\; C_h w_h \qquad\quad = \ell_{2,h} \ . \tag{3.8b}$$

Static condensation of w_h gives rise to the discrete Schur complement system

$$(S_h \;-\; \omega^2 I_h)u_h \;=\; \ell_h \ , \tag{3.9}$$

where S_h and the right-hand side ℓ_h are given by

$$S_h \;:=\; A_h + B_h C_h^{-1} B_h^* \quad , \quad \ell_h \;:=\; \ell_{1,h} + B_h C_h^{-1}\ell_{2,h}.$$

THEOREM 3.3. *Assume that ω^2 is not an eigenvalue of S as given by (3.4). Then, for sufficiently small h the discrete Schur complement system (3.9) admits a unique solution $u_h \in V_h$.*

Proof. If ω^2 is not an eigenvalue of $\mathbf{S}$, the inf-sup condition (3.6) holds true which implies

$$\begin{aligned} \beta \|u\|_V \;&\leq\; \sup_{v\in V\setminus\{0\}} \frac{|\langle (S-\omega^2 I)u, v\rangle|}{\|v\|_V} \;= \\ &= \sup_{v\in V\setminus\{0\}} \frac{|\langle (S(u-\omega^2\mathbf{S}^{-1}u), v\rangle|}{\|v\|_V} \;\leq\; \|S\|\,\|u-\omega^2 S^{-1}u\|_V. \end{aligned} \tag{3.10}$$

On the other hand, we note that S_h is the Galerkin approximation of S, i.e.,

$$\langle S_h u_h, v_h\rangle \;=\; \langle S u_h, v_h\rangle \quad , \quad u_h, v_h \in V_h \;.$$

Hence, referring to $\alpha_S > 0$ as the ellipticity constant of S, we have

$$\langle S_h v_h, v_h\rangle \;\geq\; \alpha_S \|v_h\|_V^2 \quad , \quad v_h \in V_h. \tag{3.11}$$

Using (3.11), we deduce from (3.10) that

$$\begin{aligned} &\sup_{0\neq v_h\in V_h} \frac{|\langle (S_h-\omega^2 I_h)u_h, v_h\rangle|}{\|v_h\|_V} \;=\; \sup_{0\neq v_h\in V_h} \frac{|\langle S_h(u_h-\omega^2 S_h^{-1}u_h), v_h\rangle|}{\|v_h\|_V} \\ &\geq\; \frac{|\langle S_h(u_h-\omega^2 S_h^{-1}u_h), u_h-\omega^2 S_h^{-1}u_h\rangle|}{\|u_h-\omega^2 S_h^{-1}u_h\|_V} \;\geq\; \alpha_S \|u_h-\omega^2 S_h^{-1}u_h\|_V \\ &\geq\; \alpha_S\Big(\|u_h-\omega^2 S^{-1}u_h\|_V - \omega^2\|(S_h^{-1}-S^{-1})u_h\|_V\Big) \geq\; \beta_h\,\|u_h\|_V, \end{aligned}$$

where

$$\beta_h \;:=\; \alpha_S\left(\frac{\beta}{\|S\|} - \omega^2\|S_h^{-1}-S^{-1}\|\right).$$

Since $S_h^{-1} \to S^{-1}$ as $h \to 0$, there exists $h_{max} > 0$ such that $\beta_h \geq \gamma > 0$ uniformly for $h \leq h_{max}$. This shows that $S_h - \omega^2 I_h$ asymptotically satisfies a discrete inf-sup condition which gives the assertion. ∎

The discrete saddle point problem (3.7a),(3.7b) can be written equivalently as the algebraic saddle point problem

$$\begin{pmatrix} A & B \\ B^* & -C \end{pmatrix}\begin{pmatrix} u \\ w \end{pmatrix} \;=\; \begin{pmatrix} b_1 \\ b_2 \end{pmatrix}\;, \tag{3.12}$$

where $A \in \mathbb{R}^{n_h\times n_h}, n_h := \dim \mathbf{V}_h$, and $C \in \mathbb{R}^{m_h\times m_h}, m_h := \dim W_h$, are symmetric positive definite matrices, $B \in \mathbb{R}^{n_h\times m_h}$, and $b_1 \in \mathbb{R}^{n_h}, b_2 \in \mathbb{R}^{m_h}$. The algebraic saddle point problem (3.12) can be solved by preconditioned GMRES or BiCGStab [8, 53] using an upper block-triangular preconditioner P of the form

$$P \;=\; \begin{pmatrix} \tilde{A} & \tilde{B} \\ 0 & -\tilde{C} \end{pmatrix}$$

such that

$$\gamma_A\, v^T\tilde{A}v \;\leq\; v^T A v \;\leq\; \Gamma_A\, v^T\tilde{A}v \quad , \quad \gamma_C\, w^T\tilde{C}w \;\leq\; w^T C w \;\leq\; \Gamma_C\, w^T\tilde{C}w\;,$$

with constants $0 < \gamma_A \leq \Gamma_A, 0 < \gamma_C \leq \Gamma_C$ satisfying $\Gamma_A/\gamma_A \ll \kappa(A), \Gamma_C/\gamma_C \ll \kappa(C)$, where $\kappa(A), \kappa(C)$ are the spectral radii of A and C, respectively (cf., e.g., [41]). Alternatively, preconditioned CG [9] can be applied to the Schur complement system associated with (3.12).
In practical applications, where V, W are spaces of functions on a spatial domain $\Omega \subset \mathbb{R}^d$ and $V_i, W_i, 0 \leq i \leq L$, are finite element spaces with respect to a hierarchy $\{\mathcal{T}_i\}_{i=0}^L$ of triangulations of Ω, the operators $\tilde{A}^{-1}$ and $\tilde{C}^{-1}$, needed for the implementation of the preconditioned iterative scheme, can be realized, e.g., by BPX preconditioners [20]. Corresponding results within the context of the numerical simulation of piezoelectrically actuated surface acoustic waves will be reported in the subsequent section 5.

4. Numerical Simulation of LWD (Logging-While-Drilling) Tools. LWD (Logging-While-Drilling), sometimes also referred to as MWD (Measurements-While-Drilling), are techniques for the measurement of geological formation parameters such as resistivity and porosity during the excavation of boreholes, e.g., in deepwater drilling (cf. Figure 4.1 (left)). LWD uses tools that are integrated into the BHA (Bottom-Hole Assembly). The BHA is the lower part of the drillstring which consists of the bit, a mud motor for directional drilling, stabilizers, the drill collar, and the drillpipe (cf. Figure 4.1 (right)).

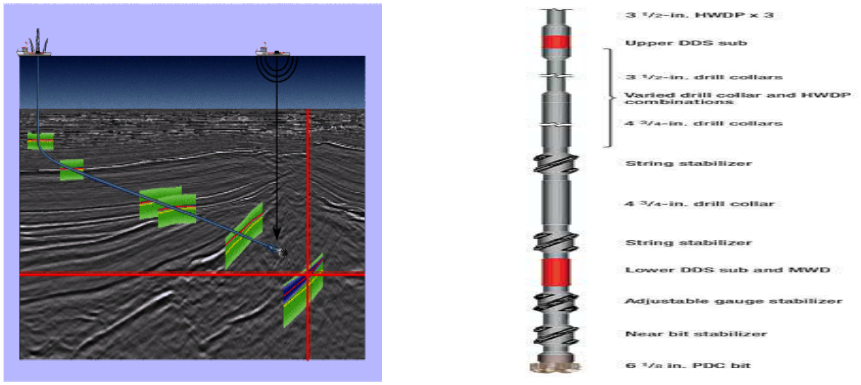

FIG. 4.1. *Horizontal deepwater drilling (l.) and a typical bottomhole assembly (r.)*

LWD tools based on an electromagnetic induction sensor are featuring saddle type transmitter and receiver antennas that are placed concentrically on a metallic mandrel (cf. Figure 4.2 (left)). The sensor is placed in the borehole with its axis being parallel to the borehole. The mandrel is a circular cylinder which is considered as a perfect electric conductor. The transmitter and receiver antennas with an aperture of 90^o are imbedded in a sleeve and protected by a magnetic shielding (cf. Figure 4.2 (right)).

The transmitter antennas carry a current of $1A$. The frequency dependence is $\exp(-2\pi i f t)$ with a frequency f up to 2 MHz. Typical dimensions of a saddle type antenna are shown in Figure 4.3 (left)). The problem to compute the open-circuit voltages features high conductivity contrasts (cf. Figure 4.3 (right)). The conductivity is 10^7 S/m in the mandrel, varies from 10 S/m to 10^{-3} S/m in the mud between the mandrel and the wall of the borehole, and ranges from 10^{-4} S/m to 10 S/m in the formation surrounding the borehole [54].

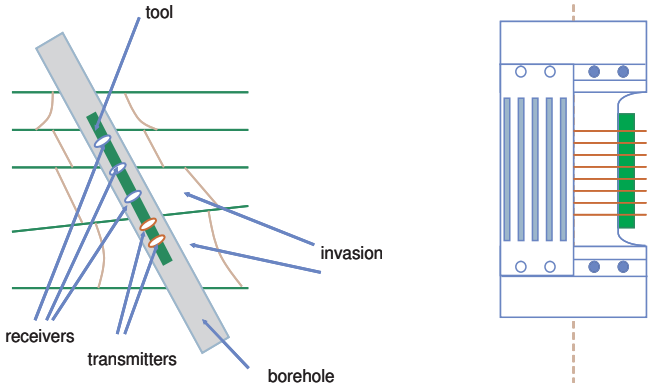

FIG. 4.2. *Schematic representations of an LWD tool with two transmitter and three receiver antennas (l.) and a typical antenna configuration (r.). Courtesy of [54].*

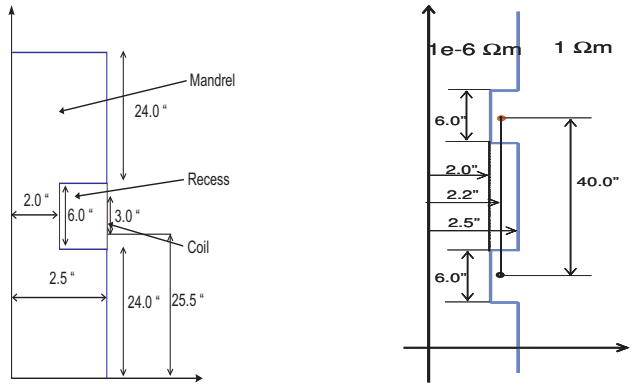

FIG. 4.3. *Schematic representations of an LWD tool with two transmitter and three receiver antennas (l.) and a typical antenna configuration (r.). Courtesy of [54].*

The computation of the geological formation parameters based on the data obtained at the receiver antennas amounts to the solution of an inverse scattering problem. Here, for an induction sensor with one transmitter and two receiver antennas we only consider part of the forward problem, namely the computation of the electric field $\mathbf{E}$ in a cylindrical domain $\Omega \subset \mathbb{R}^3$ between the mandrel and the wall of the borehole (cf. Figure 4.4).

The boundary is split according to $\Gamma = \overline{\Gamma}_1 \cup \overline{\Gamma}_2 \cup \overline{\Gamma}_3, \Gamma_1 \cap \Gamma_2 \cap \Gamma_3 = \emptyset$, where Γ_1 represents the position of the transmitter antennas, Γ_2 stands for the wall of the borehole, and $\Gamma_3 := \Gamma \setminus (\overline{\Gamma}_1 \cup \overline{\Gamma}_2)$. Assuming a time-periodic excitation, the computation of the electric field $\mathbf{E}$ requires the solution of the time-harmonic Maxwell equations:

$$\boldsymbol{\nabla}\times\mu_r^{-1}\boldsymbol{\nabla}\times\mathbf{E} - \kappa^2\varepsilon_r\mathbf{E} = \mathbf{0} \quad \text{in } \Omega, \tag{4.1a}$$

$$(\boldsymbol{\nu}\times\mathbf{E})\times\boldsymbol{\nu} = \mathbf{g}_1 \quad \text{on } \Gamma_1, \tag{4.1b}$$

$$\boldsymbol{\nu}\times(\mu_r^{-1}\boldsymbol{\nabla}\times\mathbf{E}) - i\kappa\lambda\,\boldsymbol{\nu}\times\mathbf{E} = \mathbf{g}_2 \quad \text{on } \Gamma_2, \tag{4.1c}$$

$$\boldsymbol{\nu}\times(\mu_r^{-1}\boldsymbol{\nabla}\times\mathbf{E}) = \mathbf{0} \quad \text{on } \Gamma_3. \tag{4.1d}$$

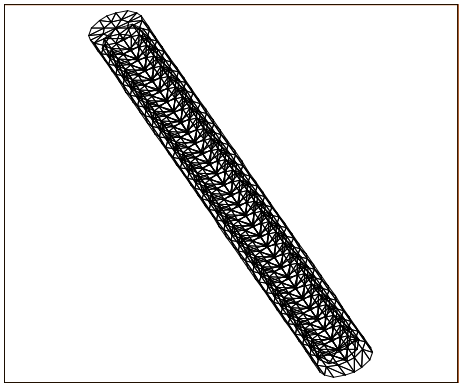

FIG. 4.4. *Computational domain consisting of the cylindrical region between the mandrel and the walls of the borehole and its initial simplicial triangulation*

Here, ε_r and μ_r stand for the relative permittivity and relative permeability

$$\varepsilon_r = \frac{1}{\varepsilon_0}\Big(\varepsilon + \frac{i\sigma}{\omega}\Big) \quad , \quad \mu_r = \frac{\mu}{\mu_0}, \tag{4.2}$$

where ε, μ denote the permittivity and permeability of the medium and ε_0, μ_0 are the permittivity and permeability in vacuum. Moreover, σ refers to the conductivity and κ stands for the wavenumber $\kappa = \omega\sqrt{\varepsilon_0\mu_0}$, where $\omega = 2\pi f$ is the angular frequency. Finally, λ is given by

$$\lambda = (1+i)\sqrt{\frac{\pi\sigma}{\omega\mu}}, \tag{4.3}$$

and $\boldsymbol{\nu}$ stands for the unit exterior normal vector on Γ. The tangential vector fields $\mathbf{g}_1$ and $\mathbf{g}_2$ are assumed to be given on Γ_1 and Γ_2, respectively. We refer to [45] for the derivation of (4.1a)-(4.1d) from Maxwell's equations.
As in section 2, we denote by $\mathbf{H}(\mathbf{curl};\Omega)$ the Hilbert space of complex-valued vector fields $\mathbf{q}$ with components in $L^2(\Omega)$ such that the components of $\boldsymbol{\nabla}\times\mathbf{q}$ also live in $L^2(\Omega)$, equipped with the standard graph norm $\|\cdot\|_{curl,\Omega}$. We recall that the space $\mathbf{H}^{-1/2}(\mathbf{curl}_{\Gamma_i};\Gamma_i)$ is the trace space of tangential component traces $(\boldsymbol{\nu}\times\mathbf{q})\times\boldsymbol{\nu}$ on Γ_i, whereas the space $\mathbf{H}^{-1/2}(\mathbf{curl}_{\Gamma_i};\Gamma_i)$ stands for the trace space of tangential traces $\boldsymbol{\nu}\times\mathbf{q}$ on Γ_2. Here, $\mathbf{curl}_{\Gamma_i}$ and div_{Γ_i} are the surfacic divergence and surfacic rotation, respectively (cf., e.g., [23]). Assuming

$$\mathbf{g}_1 \in \mathbf{H}^{-1/2}(\mathbf{curl}_{\Gamma_1};\Gamma_1) \quad , \quad \mathbf{g}_2 \in \mathbf{H}^{-1/2}(\mathrm{div}_{\Gamma_2};\Gamma_2), \tag{4.4}$$

we set

$$\mathbf{V} := \{\mathbf{q} \in \mathbf{H}(\mathbf{curl};\Omega) \mid \mathbf{q}\times\boldsymbol{\nu}|_{\Gamma_1} = \mathbf{g}_1\} \quad , \quad \mathbf{V_0} := \{\mathbf{q} \in \mathbf{H}(\mathbf{curl};\Omega) \mid \mathbf{q}\times\boldsymbol{\nu}|_{\Gamma_1} = \mathbf{0}\}.$$

The weak formulation of (4.1a)-(4.1d) is to find $\mathbf{E} \in \mathbf{V}$ such that

$$a_\Omega(\mathbf{E},\mathbf{q}) + b_{\Gamma_2}(\mathbf{E},\mathbf{q}) = \ell(\mathbf{q}) \quad , \quad \mathbf{q} \in \mathbf{V_0}. \tag{4.5}$$

Here, the sesquilinear forms $a_\Omega(\cdot,\cdot)$, $b_{\Gamma_2}(\cdot,\cdot)$, and the functional $\ell(\cdot)$ are given by

$$a_\Omega(\mathbf{E},\mathbf{q}) := \int_\Omega \Big(\mu_r^{-1}(\boldsymbol{\nabla}\times\mathbf{E})\cdot(\boldsymbol{\nabla}\times\mathbf{q}) - (\kappa^2\varepsilon_r + i\omega\sigma)\mathbf{E}\cdot\mathbf{q}\Big)\, d\mathbf{x},$$

$$b_{\Gamma_2}(\mathbf{E},\mathbf{q}) := \langle i\kappa\lambda\boldsymbol{\nu}\times\mathbf{E}, (\boldsymbol{\nu}\times\mathbf{q})\times\boldsymbol{\nu}\rangle_{\Gamma_2} \quad , \quad \ell(\mathbf{q}) := \langle \mathbf{g}_2, (\boldsymbol{\nu}\times\mathbf{q})\times\boldsymbol{\nu}\rangle_{\Gamma_2},$$

where $\langle\cdot,\cdot\rangle_{\Gamma_2}$ is the dual pairing between $\mathbf{H^{-1/2}}(\mathrm{div}_{\Gamma_2};\Gamma_2)$ and $\mathbf{H^{-1/2}}(\mathbf{curl}_{\Gamma_2};\Gamma_2)$. For sufficiently regular data of the problem, it is well-known that if κ is not an eigenvalue of the associated Maxwell eigenproblem, then the variational equation (4.5) has a unique solution $\mathbf{E}\in\mathbf{V}$ (cf., e.g., [45]).
Given a simplicial triangulation $\mathcal{T}_h(\Omega)$ of the computational domain Ω that aligns with the partition of the boundary Γ, we discretize (4.5) by the lowest order edge elements

$$\mathbf{Nd^1}(T) := \{\mathbf{q} \mid \mathbf{q}(\mathbf{x}) = \mathbf{a} + \mathbf{b}\times\mathbf{x}\ ,\ \mathbf{a},\mathbf{b}\in\mathbb{R}^3\},$$

of Nédélec's first family [48] with the degrees of freedom given by zero order moments of the tangential trace components on the six edges of $T\in\mathcal{T}_h(\Omega)$. We refer to

$$\mathbf{Nd^1}(\Omega;\mathcal{T}_h(\Omega)) := \{\mathbf{q}_h\in\mathbf{H}(\mathbf{curl};\Omega) \mid \mathbf{q}|_T\in\mathbf{Nd^1}(T)\ ,\ T\in\mathcal{T}_h(\Omega)\}$$

as the associated curl-conforming edge element space. Assuming $\mathbf{g}_{1,h}\in\mathbf{L}^2(\Gamma_1)$ and $\mathbf{g}_{2,h}\in\mathbf{L}^2(\Gamma_2)$ to be appropriately chosen approximations of $\mathbf{g_1}$ and $\mathbf{g_2}$, we set

$$\mathbf{V}_h := \{\mathbf{q}_h\in\mathbf{Nd^1}(\Omega;\mathcal{T}_h(\Omega)) \mid (\boldsymbol{\nu}\times\mathbf{q}_h)\times\boldsymbol{\nu}|_{\Gamma_1} = \mathbf{g}_{1,h}\} \quad , \quad \mathbf{V}_{h,0} := \quad \mathbf{V}_h\cap\mathbf{V_0},$$

and consider the following edge element approximation of (4.5): Find $\mathbf{E}_h\in\mathbf{V}_h$ such that

$$a_{h,\Omega}(\mathbf{E}_h,\mathbf{q}_h) + b_{h,\Gamma_2}(\mathbf{E}_h,\mathbf{q}_h) = \ell_h(\mathbf{q}_h) \quad , \quad \mathbf{q}_h\in\mathbf{V}_{h,0}. \tag{4.6}$$

Here, the sequilinear forms $a_{h,\Omega}(\cdot,\cdot), b_{h,\Gamma_2}(\cdot,\cdot)$, and the functional $\ell_h(\cdot)$ are given by

$$\begin{aligned}
a_{h,\Omega}(\mathbf{E}_h,\mathbf{q}_h) &:= \sum_{T\in\mathcal{T}_h(\Omega)}\int_T \Big(\mu_r^{-1}(\boldsymbol{\nabla}\times\mathbf{E}_h)\cdot(\boldsymbol{\nabla}\times\mathbf{q}_h) - (\kappa^2\varepsilon_r + i\omega\sigma)\mathbf{E}_h\cdot\mathbf{q}_h\Big)\ d\mathbf{x},\\
b_{h,\Gamma_2}(\mathbf{E}_h,\mathbf{q}_h) &:= \sum_{F\in\mathcal{F}_h(\Gamma_2)}\int_F i\kappa\lambda\boldsymbol{\nu}\times\mathbf{E}_h\cdot((\boldsymbol{\nu}\times\mathbf{q}_h)\times\boldsymbol{\nu})\ d\boldsymbol{\tau},\\
\ell_h(\mathbf{q}_h) &:= \sum_{F\in\mathcal{F}_h(\Gamma_2)}\int_F \mathbf{g}_{h,2}\cdot((\boldsymbol{\nu}\times\mathbf{q}_h)\times\boldsymbol{\nu})\ d\boldsymbol{\tau}.
\end{aligned}$$

We have solved (4.6) by local multigrid with local Hiptmair-Gauss-Seidel smoothing (V-cycle, one pre- and one post-smoothing step) using a hierarchy of four tetrahedral meshes ($L=3$) created by local refinement on the basis of weighted residual-type a posteriori error estimators. The error estimator consists of weighted element residuals

$$\begin{aligned}
\eta_{T,1}^2 &:= \alpha_{T,1}\ h_T^2\ \|\boldsymbol{\nabla}\times(\mu_r^{-1}\boldsymbol{\nabla}\times\mathbf{E}_h) - \kappa^2\varepsilon_r\mathbf{E}_h\|_{0,T}^2 \quad , \quad T\in\mathcal{T}_h(\Omega),\\
\eta_{T,2}^2 &:= \alpha_{T,2}\ h_T^2\ \|\kappa^2\ \boldsymbol{\nabla}\cdot\varepsilon_r\mathbf{E}_h\|_{0,T}^2 \quad , \quad T\in\mathcal{T}_h(\Omega),
\end{aligned}$$

and weighted face residuals

$$\begin{aligned}
\eta_{F,1}^2 &:= \alpha_{F,1}\ h_F\ \|[\boldsymbol{\nu}\times(\mu_r^{-1}\ \boldsymbol{\nabla}\times\mathbf{E}_h]_F\|_{0,F}^2 \quad , \quad F\in\mathcal{F}_h(\Omega),\\
\eta_{F,2}^2 &:= \alpha_{F,2}\ h_F\ \|\kappa^2\ [\boldsymbol{\nu}\cdot(\varepsilon_r\mathbf{E}_h)]\|_{0,F}^2 \quad , \quad F\in\mathcal{F}_h(\Omega),\\
\eta_{F,3}^2 &:= \alpha_{F,3}\ h_F\ \|\mathbf{g}_{1,h} - (\boldsymbol{\nu}\times\mathbf{E}_h)\times\boldsymbol{\nu}\|_{0,F}^2 \quad , \quad F\in\mathcal{F}_h(\Gamma_1),\\
\eta_{F,4}^2 &:= \alpha_{F,4}\ h_F\ \|\mathbf{g}_{2,h} - \Big(\boldsymbol{\nu}\times(\mu_r^{-1}\boldsymbol{\nabla}\times\mathbf{E}_h) - i\kappa\ \lambda\ \boldsymbol{\nu}\times\mathbf{E}_h\Big)\|_{0,F}^2 \quad , \quad F\in\mathcal{F}_h(\Gamma_2),
\end{aligned}$$

where $[\cdot,\cdot]_F$ stands for the jump across interior faces. We have chosen different weights $\alpha_{T,k}, 1 \leq k \leq 2$, and $\alpha_{F,k}, 1 \leq k \leq 4$, for the element and face residuals in the regions around the transmitter antenna and the receiver antennas to ensure a proper resolution, since the electric field is significantly smaller in the vicinity of the receiver antennas. The initial coarse triangulation of the computational domain is shown in Figure 4.4. Figure 4.5 shows the adaptively refined mesh on the metallic mandrel around the coils of the transmitter antenna (left) and in the region around the aperture (right). We observe a pronounced local refinement in these regions. Figure 4.6 displays the computed electric field $\mathbf{E}_h$ (left) and the computed magnetic induction $\mathbf{B}_h$ (right) in a vicinity of the transmitter antenna along with the adaptively refined mesh. The fields are restricted to the recess around the coils and, as expected, rapidly decay off the transmitter antenna.

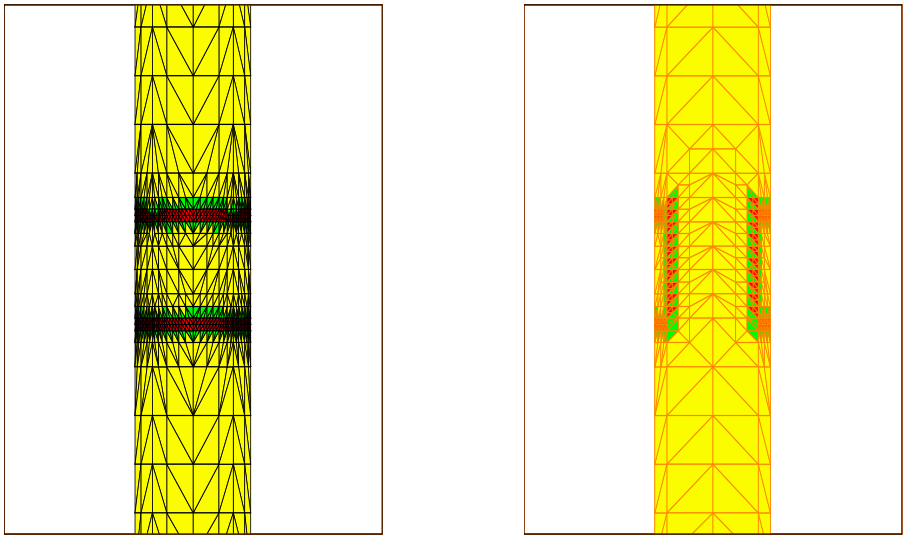

FIG. 4.5. *Adaptively refined mesh on the mandrel around the coils of the transmitter antenna (l.) and around the aperture (r.)*

5. Numerical Simulation of Piezoelectrically Actuated Surface Acoustic Waves (SAW). Piezoelectric materials are able to generate an electric field in response to an applied mechanical stress which is called the direct piezoelectric effect. The reverse piezoelectric effect is the generation of a mechanical stress and strain under the influence of an applied electric field. The origin of both effects is related to an asymmetry in the unit cell of a piezoelectric crystal which causes a change in the polarization density. It can be observed only in materials with a polar axis (cf., e.g., [30, 42]). Here, we are interested in the simulation of piezoelectrically actuated surface acoustic waves [33, 34] with applications in signal processing [28, 31, 40, 46] and life sciences [5, 6, 32, 60, 61].
In piezoelectric materials, the stress tensor $\boldsymbol{\sigma}$ depends linearly on the electric field $\mathbf{E}$ according to a generalized Hooke's law

$$\boldsymbol{\sigma}(\mathbf{u},\mathbf{E}) \;=\; \mathbf{c}\,\boldsymbol{\varepsilon}(\mathbf{u}) \;-\; \mathbf{e}\,\mathbf{E}\,. \tag{5.1}$$

Here, $\mathbf{u}$ denotes the mechanical displacement vector and $\boldsymbol{\varepsilon}(\mathbf{u}) := (\nabla\mathbf{u} + (\nabla\mathbf{u})^T)/2$ stands for the linearized strain tensor. Moreover, $\mathbf{c}$ and $\mathbf{e}$ are the symmetric fourth

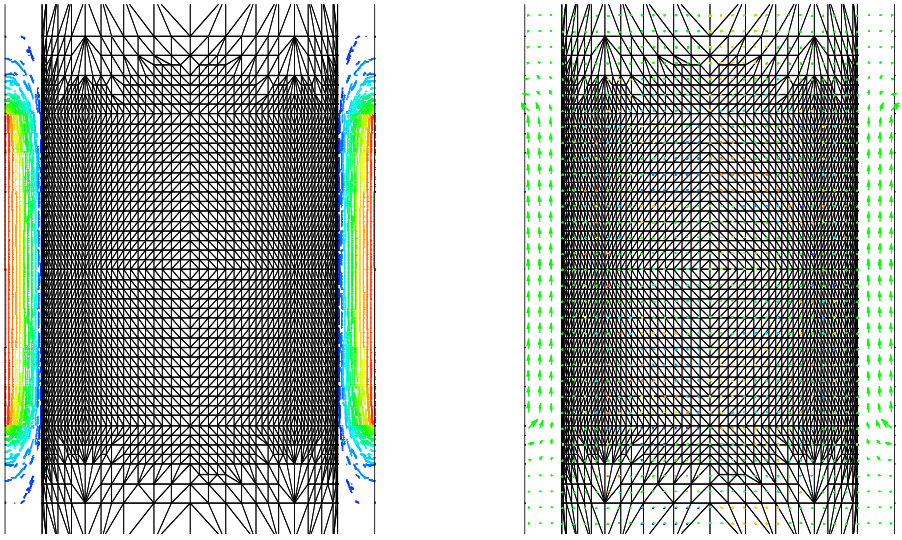

FIG. 4.6. *Computed electric field (l.) and magnetic induction (r.) in a vicinity of the transmitter antenna*

order elasticity tensor and the symmetric third order piezoelectric tensor. Since the frequency of the applied electromagnetic wave is small compared to the frequency of the generated acoustic wave, a coupling can be neglected. Moreover, the electric field is irrotational. Consequently, it can be expressed as the gradient of an electric potential Φ according to $\mathbf{E} = -\nabla\Phi$. Since piezoelectric materials are nearly perfect insulators, the only remaining quantity of interest in Maxwell's equations is the dielectric displacement $\mathbf{D}$ which is related to the electric field by the constitutive equation

$$\mathbf{D} \;=\; \boldsymbol{\epsilon}\,\mathbf{E} \;+\; \mathbf{P}\;, \tag{5.2}$$

where $\boldsymbol{\epsilon}$ is the permittivity of the material and $\mathbf{P}$ stands for the polarization. In piezoelectric materials, the polarization $\mathbf{P}$ is linear, i.e., there holds

$$\mathbf{P} \;=\; \mathbf{e}\,\boldsymbol{\varepsilon}(\mathbf{u})\;. \tag{5.3}$$

We assume that the piezoelectric material with density $\rho > 0$ occupies some rectangular domain Ω with boundary $\Gamma = \partial\Omega$ and exterior unit normal $\boldsymbol{\nu}$ such that

$$\begin{aligned}
\Gamma = \overline{\Gamma}_{E,D} \cup \overline{\Gamma}_{E,N} \quad &, \quad \Gamma_{E,D} \cap \Gamma_{E,N} = \emptyset\;, \\
\Gamma = \overline{\Gamma}_{p,D} \cup \overline{\Gamma}_{p,N} \quad &, \quad \Gamma_{p,D} \cap \Gamma_{p,N} = \emptyset\;,
\end{aligned}$$

where $\Gamma_{E,D}$ is a rectangular subdomain of the upper boundary of Γ and $\Gamma_{E,N} := \Gamma \setminus \overline{\Gamma}_{E,D}$. Given boundary data $\Phi_{E,D}$ on $\Gamma_{E,D}$, the pair $(\mathbf{u}, \Phi)$ satisfies the following

initial-boundary value problem for the piezoelectric equations

$$\rho\,\frac{\partial^2 \mathbf{u}}{\partial t^2} \;-\; \boldsymbol{\nabla}\cdot\boldsymbol{\sigma}(\mathbf{u},\mathbf{E}) \;=\mathbf{0} \quad \text{in } Q := \Omega\times(0,T)\;, \tag{5.4a}$$

$$\boldsymbol{\nabla}\cdot\mathbf{D}(\mathbf{u},\mathbf{E}) \;=0 \quad \text{in } Q\;, \tag{5.4b}$$

$$\mathbf{u} \;=\; 0 \quad \text{on } \Gamma_{p,D} \quad,\quad \boldsymbol{\nu}\cdot\boldsymbol{\sigma} \;=\boldsymbol{\sigma}_{\boldsymbol{\nu}} \text{ on } \Gamma_{p,N}\;, \tag{5.4c}$$

$$\Phi \;=\; \Phi_{E,D} \quad \text{on } \Gamma_{E,D} \quad,\quad \boldsymbol{\nu}\cdot\mathbf{D} \;=D_{\boldsymbol{\nu}} \text{ on } \Gamma_{E,N}\;, \tag{5.4d}$$

$$\mathbf{u}(\cdot,0) \;=\; 0 \quad,\quad \frac{\partial \mathbf{u}}{\partial t}(\cdot,0) \;=0 \quad \text{in } \Omega\;. \tag{5.4e}$$

These equations have to be completed by the constitutive equations (5.1),(5.2) and (5.3). Assuming time periodic excitations $\Phi_{E,D}(\cdot,t) = \mathrm{Re}\left(\hat{\Phi}_{E,D}\exp(-\,i\omega t)\right)$ such that $\hat{\Phi}_{E,D}\in H^{1/2}(\Gamma_{E,D})$, we are looking for time harmonic solutions

$$\mathbf{u}(\cdot,t) \;=\; \mathrm{Re}\,(\,\mathbf{u}(\cdot)\exp(-\,i\omega t)\,) \quad,\quad \Phi(\cdot,t) \;=\; \mathrm{Re}\,(\,\Phi(\cdot)\exp(-\,i\omega t)\,)\;.$$

This leads to a saddle point problem for a Helmholtz-type equation which in its weak form amounts to the computation of $(\mathbf{u},\Phi)\in\mathbf{V}\times W$, where $\mathbf{V}_0 := H^1_{0,\Gamma_{p,D}}(\Omega)^3$ and $W := \{\varphi\in H^1(\Omega)\mid \varphi_{\Gamma_{E,D}} = \hat{\Phi}_{E,D}\}$, such that for all $\mathbf{v}\in\mathbf{V}$ and $\psi\in W_0 := H^1_{0,\Gamma_{E,D}}(\Omega)$

$$a(\mathbf{u},\mathbf{v}) \;+\; b(\Phi,\mathbf{v}) \;-\; \omega^2\rho\;(\mathbf{u},\mathbf{v})_{0,\Omega} \;=\ell_1(\mathbf{v})\;, \tag{5.5a}$$

$$b(\psi,\mathbf{u}) \;-\; c(\Phi,\psi) \;=\ell_2(\psi)\;. \tag{5.5b}$$

Here,

$$H^1_{0,\Gamma_{p,D}}(\Omega)^3 := \{\mathbf{v}\in H^1(\Omega)^3 \mid \mathbf{v}|_{\Gamma_{p,D}} = 0\},$$
$$H^1_{0,\Gamma_{E,D}}(\Omega) := \{\psi\in H^1(\Omega) \mid \psi_{\Gamma_{E,D}} = 0\},$$

and the sesquilinear forms $a(\cdot,\cdot), b(\cdot,\cdot), c(\cdot,\cdot)$ and the functionals $\ell_1\in\mathbf{V}^*, \ell_2\in W^*$ are given by

$$a(\mathbf{v},\mathbf{w}) \;:=\; \int_\Omega \mathbf{c}\,\boldsymbol{\varepsilon}(\mathbf{v}) : \boldsymbol{\varepsilon}(\bar{\mathbf{w}})\;d\mathbf{x} \quad,\quad b(\varphi,\mathbf{v}) \;:=\; \int_\Omega \mathbf{e}\,\nabla\varphi : \boldsymbol{\varepsilon}(\bar{\mathbf{v}})\;d\mathbf{x}\;,$$

$$c(\varphi,\psi) := \int_\Omega \boldsymbol{\epsilon}\,\nabla\varphi\cdot\nabla\bar{\psi}\;d\mathbf{x}\;,$$

$$\ell_1(\mathbf{v}) \;:=\; \langle\boldsymbol{\sigma}_{\mathbf{n}_1},\mathbf{v}\rangle_{p,N} \quad,\quad \ell_2(\psi) \;:=\; \langle D_{\mathbf{n}_1},\psi\rangle_{E,N}\;,$$

with $\langle\cdot,\cdot\rangle_{p,N}, \langle\cdot,\cdot\rangle_{E,N}$ denoting the dual pairings between the associated trace spaces and their dual spaces, respectively.
The saddle point problem (5.5a),(5.5b) satisfies the assumptions of Theorem 3.1 of section 3. Hence, if ω is not an eigenvalue of the associated eigenvalue problem, there exists a unique solution $(\mathbf{u},\Phi)\in\mathbf{V}\times W$.

We have performed numerical simulations of SAWs for plates of length L, width W, and height H such that $\Omega_1 := (0,L)\times(0,W)\times(0,H)$ with $\Gamma_{p,D} := [0,L]\times[0,W]\times\{0\}$. As the piezoelectric material we have assumed Lithiumniobate ($LiNbO_3$). Table 5.1 contains the elasticity tensor $\mathbf{c}$, the piezoelectric tensor $\boldsymbol{\varepsilon}$, the electric permittivity tensor $\boldsymbol{\epsilon}$, and the density ρ_p of this material.

TABLE 5.1
Piezoelectric material moduli (Lithiumniobate $LiNbO_3$)

Elast. tensor $\mathbf{10^{10}\,\frac{N}{m^2}}$	$c_{11}=c_{22}$ 20.3	c_{12} 5.3	$c_{13}=c_{23}$ 7.5	$c_{14}=-c_{24}=c_{56}$ 0.9	c_{33} 24.5	$c_{44}=c_{55}$ 6.0	c_{66} 7.5
Piezoel. tensor $\frac{C}{m^2}$	$e_{15}=e_{24}$ 3.7		$e_{22}=-e_{21}=-e_{16}$ 2.5		$e_{31}=e_{32}$ 0.1		e_{33} 1.3
Permitt. tensor $10^{-12}\,\frac{F}{m}$	$\epsilon_{11}=\epsilon_{22}$ 749.0		ϵ_{33} 253.2	**Density** $10^3\,\frac{kg}{m^3}$		ρ_p 4.63	

The IDT has been positioned at the top of the plate, i.e., $\Gamma_{E,D} := [L_1, L_2] \times [W_1, W_2] \times \{L\}$, and has been assumed to operate at a frequency $\omega/(2\pi) = 100\,MHz$ thus generating SAWs of wavelength $\lambda = 40\,\mu m$. In order to control the finite element error appropriately, following [39] we have chosen an initial mesh of mesh length $h \lesssim \sqrt{\lambda^3}$.
For a plate of length $L = 1.2\,mm$, width $W = 0.6\,mm$, height $H = 0.6\,mm$, and $\Gamma_{E,D} := [0.2, 0.4] \times [0.1, 0.5] \times \{1.2\}$, Figure 5.1 (left) shows the computed amplitudes of the electric potential wave for the longitudinal section $[0, 1.2] \times \{0.3\} \times [0, 0.6]$.

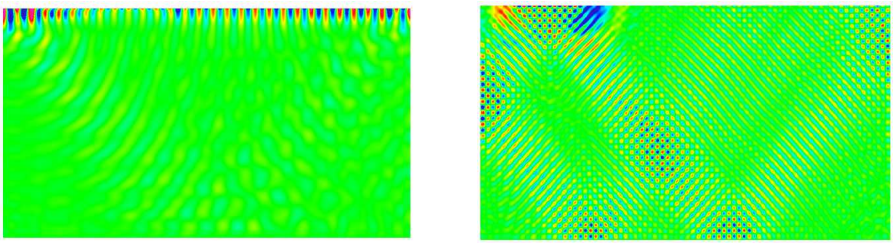

FIG. 5.1. *Amplitudes of a surface acoustic wave (100 MHz) (l.) and bulk wave (200 MHz) (r.)*

As can be clearly seen, the SAWs are strictly confined to the surface of the piezoelectric material with a penetration depth of approximately one wavelength as it is required for their application in nano-pumps for SAW driven microfluidic biochips. The SAW velocity is $4.0 \cdot 10^3\,m/s$. In contrast to this, Figure 5.1 (right) displays a typical bulk wave generated by an IDT operating at a frequency of 200 MHz which ia a wave configuration useful for applications in telecommunications (cell phones).

For a simplified test case from [32], Table 5.2 and Table 5.3 reflect the convergence histories of the iterative schemes without and with the BPX-type preconditioner.

TABLE 5.2
Number of iterations and CPU-time (in seconds) for SC-CG and BICGSTAB/GMRES without using a preconditioner

Level	SC-CG		BICGSTAB		GMRES	
	time	iter	time	iter	time	iter
3	0.15	74	0.10	65	0.14	17
4	1.4	148	0.75	137	1.7	56
5	29	311	7.6	324	32	206
6	440	872	75	678	530	758

TABLE 5.3
Number of iterations and CPU-time (in seconds) for SC-PCG and BICGSTAB/GMRES with a block-diagonal preconditioner

Level	SC-PCG		PBICGSTAB		PGMRES	
	time	iter	time	iter	time	iter
5	2.5	48	1.1	33	1.2	6
6	12	52	5.2	39	5.9	7
7	70	55	23	41	25	7
8	290	57	92	44	100	8

REFERENCES

[1] M. Ainsworth and W. McLean, Multilevel diagonal scaling preconditioners for boundary element equations on locally refined meshes. Numer. Math. **93**, 387-413, 2003.

[2] M. Ainsworth and J.T. Oden, A Posteriori Error Estimation in Finite Element Analysis. John Wiley & Sons, Inc., New York, 2000.

[3] B. Aksoylu, S. Bond, and M. Holst, An odyssee into local refinement and multilevel preconditioning III: implementation and numerical experiments. SIAM J. Sci. Comput. **25**, 478-498, 2003.

[4] B. Aksoylu and M. Holst, Optimality of multilevel preconditioners for local mesh refinement in three dimensions. SIAM J. Numer. Anal. **44**, 1005-1025, 2006.

[5] H. Antil, A. Gantner, R.H.W. Hoppe, D. Köster, K.G. Siebert, and A. Wixforth, Modeling and simulation of piezoelectrically agitated acoustic streaming on microfluidic biochips. In: Proc. 17th Int. Conf. on Domain Decomposition Methods (Langer, U. et al.; eds.), Lecture Notes in Computational Science and Engineering, Vol. 60, pp. 305–312, Springer, Berlin Heidelberg-New York, 2007.

[6] H. Antil, R. Glowinski, R.H.W. Hoppe, C. Linsenmann, T.W. Pan, and A. Wixforth, Modeling, simulation, and optimization of surface acoustic wave driven microfluidic biochips. J. Comp. Math. **28**, 149–169, 2010.

[7] D. Arnold, R. Falk, and R. Winther, Multigrid in H(div) and H(curl). Numer. Math. **85**, 197–218, 2000.

[8] O. Axelsson, Iterative Solution Methods. Cambridge University Press, Cambridge, 1996.

[9] O. Axelsson and L.Y. Kolotilina (Eds.), Preconditioned Conjugate Gradient Methods. Springer, Berlin-Heidelberg-New York, 2008.

[10] I. Babuska and T. Strouboulis, The Finite Element Method and its Reliability. Clarendon Press, Oxford, 2001.

[11] D. Bai and A. Brandt, Local mesh refinement multilevel techniques. SIAM J. Sci. Stat. Comput. **8**, 109-134, 1987.

[12] E. Bänsch, Local mesh refinement in 2 and 3 dimensions. Impact of Computing in Science and Engineering **3**, 181-191, 1991.

[13] W. Bangerth and R. Rannacher, Adaptive Finite Element Methods for Differential Equations. Lectures in Mathematics. ETH-Zürich. Birkhäuser, Basel, 2003.

[14] R. Beck, R. Hiptmair, R.H.W. Hoppe, and B. Wohlmuth, Residual based a posteriori error estimators for eddy current computation. M^2AN Math. Modeling and Numer. Anal. **34**, 159–182, 2000.

[15] P. Binev, W. Dahmen, and R. DeVore, Adaptive finite element methods with convergence rates. Numer. Math. **97**, 219-268, 2004.

[16] D. Braess and W. Hackbusch, A new convergence proof for the multigrid method including the V-cycle. SIAM J. Numer. Anal. **36**, 967-975, 1983.

[17] J.H. Bramble, Multigrid methods. Pitman, Boston, 1993.

[18] J.H. Bramble and J.E. Pasciak, New estimates for multigrid algorithms including the

V-cycle. Math. Comp. **60**, 447-471, 1993.
[19] J.H. Bramble, J.E. Pasciak, J.Wang, and J. Xu, Convergence estimates for product iterative methods with applications to domain decomposition. Math. Comp. **57**, 23-45, 1991.
[20] J.H. Bramble, J.E. Pasciak, and J. Xu, Parallel multilevel preconditioners. Math. Comp., **55**, 1–22, 1990.
[21] S.C. Brenner, Convergence of the multigrid V-cycle algorithms for the second order boundary value problems without full elliptic regularity. Math. Comp. **71**, 507-525, 2002.
[22] F. Brezzi and M. Fortin, Mixed and Hybrid Finite Element Methods. Springer, Berlin-Heidelberg-New York, 1991.
[23] A. Buffa, M. Costabel, and D. Sheen, On traces for $H(curl, \Omega)$ in Lipschitz domains, J. Math. Anal. Appl. **276**, 845–867, 2002.
[24] C. Carstensen and R.H.W. Hoppe, Convergence analysis of an adaptive edge finite element method for the 2d eddy current equations. J. Numer. Math. **13**, 19–32, 2005.
[25] J.M. Cascon, C. Kreuzer, R.H. Nochetto, and K.G. Siebert, Quasi-optimal convergence rate for an adaptive finite element method. SIAM J. Numer. Anal. **46**, 2524-2550, 2008.
[26] P.G. Ciarlet, The Finite Element Method for Elliptic Problems. SIAM, Philadaelphia, 2002.
[27] W. Dahmen and A. Kunoth, Multilevel preconditioning. Numer. Math. **63**, 315-344, 1992.
[28] R.W. Eason and A. Miller, Nonlinear Optics in Signal Processing. Chapman & Hall, London, 1993.
[29] K. Eriksson, D. Estep, P. Hansbo, and C. Johnson, Computational Differential Equations. Cambridge University Press, Cambridge, 1996.
[30] A.C. Eringen and G.A. Maugin, Electrodynamics of Continua I. Foundations and Solid Media. Springer, Berlin-Heidelberg-New York, 1990.
[31] M. Feldmann and J. Hénaff, Surface Acoustic Waves for Signal Processing. Artech House, Boston, 1989.
[32] A. Gantner, R.H.W. Hoppe, D. Köster, K.G. Siebert, and A. Wixforth, Numerical simulation of piezoelectrically agitated surface acoustic waves on microfluidic biochips. Comp. Visual. Sci. **10**, 145-161, 2007.
[33] J.G. Gualtieri, J.A. Kosinski, and A. Ballato, Piezoelectric materials for acoustic wave applications. IEEE Trans. Ultrasonics, Ferroelectrics, and Frequency Control **41**, 53–59, 1994.
[34] P. Günter and J.-P. Huignard (Eds.), Photorefractive Materials and Their Applications 1. Basic Effects. Springer, Berlin-Heidelberg-New York, 2006.
[35] W. Hackbusch, Multigrid Methods and Applications. Springer, Berlin-Heidelberg-New York, 1985.
[36] R. Hiptmair, Multigrid method for Maxwell's equations. SIAM J. Numer. Anal. **36**, 204-225, 1998.
[37] R. Hiptmair, Finite elements in computational electromagnetism. Acta Numerica **11**, 237-339, 2002.
[38] R.H.W. Hoppe and J. Schöberl, Convergence of adaptive edge element methods for the 3D eddy currents equations. J. Comp. Math. **27**, 657–676, 2009.
[39] F. Ihlenburg, Finite Element Analysis of Acoustic Scattering. Springer, New York, 1998.
[40] G.S. Kino, Acoustic Waves: Devices, Imaging, and Analog Signal Processing. Prentice-Hall, Englewood Cliffs, 1987.
[41] A. Klawonn, An optimal preconditioner for a class of saddle point problems with a penalty term. SIAM J. Sci. Comput. **19**, 540–552, 1998.
[42] G.A. Maugin, Continuum Mechanics of Electromagnetic Solids. North-Holland, Amsterdam, 1987.

[43] S. McCormick, Multilevel Adaptive Methods for Partial Differential Equations. Frontiers in Applied Math., Vol. 6, SIAM, Philadelphia, 1989.
[44] W.F. Mitchell, Optimal multilevel iterative methods for adaptive grids. SIAM J. Sci. Stat. Comput. **13**, 146-167, 1992.
[45] P. Monk, Finite Element Methods for Maxwell's equations. Clarendon Press, Oxford, 2003.
[46] D.P. Morgan, Surface-Wave Devices for Signal Processing. Elsevier, Amsterdam, 1991.
[47] P. Morin, R.H. Nochetto, and K.G. Siebert, Convergence of adaptive finite element methods. SIAM Review, **44**, 631-658, 2002.
[48] J.C. Nédélec, Mixed finite elements in $\mathbb{R}^3$. Numer. Math. **35**, 315–341, 1980.
[49] P. Neittaanmäki and S. Repin, Reliable methods for mathematical modelling. Error control and a posteriori estimates. Elsevier, New York, 2004.
[50] P. Oswald, Multilevel Finite Element Approximation: Theory and Applications. Teubner, Stuttgart, 1994.
[51] A. Quarteroni and A. Valli, Domain Decomposition Methods for Partial Differential Equations. Clarendon Press, Oxford, 1999.
[52] U. Rüde, Fully adaptive multigrid methods. SIAM J. Numer. Anal. **30**, 230-248, 1993.
[53] Y. Saad, Iterative Methods for Sparse Linear Systems. Cambridge University Press, Cambridge, 2003.
[54] Schlumberger Oilfield Services, Private communication. Sugarland, TX, 2010.
[55] B.F. Smith, P.E. Bjørstad, and W.D. Gropp, Domain Decomposition Methods. Cambridge University Press, Cambridge, 1996.
[56] R. Stevenson, Optimality of a standard adaptive finite element method. Foundations of Computional Mathematics **2**, 245-269, 2007.
[57] A. Toselli and O. Widlund, Domain Decomposition Methods - Algorithms and Theory. Springer, Berlin-Heidelberg-New York, 2005.
[58] U. Trottenberg, K. Oosterlee, and A. Schüller, Multigrid. Academic Press, New York, 2000.
[59] R. Verfürth, A Review of A Posteriori Error Estimation and Adaptive Mesh-refinement Techniques. Wiley-Teubner, Chichester, 1996.
[60] A. Wixforth, Acoustically driven programmable microfluidics for biological and chemical applications. JALA **11**, 399-405, 2006.
[61] A. Wixforth, C. Strobl, C. Gauer, A. Toegl, J. Scriba, and Z. Guttenberg, Acoustic manipulation of small droplets. Anal. Bioanal. Chem. **379**, 982-991, 2004.
[62] H.J. Wu and Z.M. Chen, Uniform convergence of multigrid V-cycle on adaptively refined finite element meshes for second order elliptic problems. Science in China **39**, 1405-1429, 2006.
[63] O.B. Widlund, Optimal iterative refinement methods. In: Domain Decomposition Methods, T. Chan, R. Glowinski, J. Périaux, and O. Widlund, eds., pp. 114-125, SIAM, Philadelphia, 1989.
[64] J. Xu, Iterative methods by space decomposition and subspace correction. SIAM Review **34**, 581-613, 1992.
[65] J. Xu and L. Zikatanov, The method of alternating projections and the method of subspace corrections in Hilbert space. J.Amer.Math.Soc. **15**, 573-597, 2002.
[66] X. Xu, H. Chen, and R.H.W. Hoppe, Optimality of local multilevel methods on adaptively refined meshes for elliptic boundary value problems. J. Numer. Math. **18**, No. 1 (in press), 2010.
[67] H. Yserentant, On the multi-level splitting of finite element spaces. Numer. Math., **49**, 379-412, 1986.
[68] H. Yserentant, Two preconditioners based on the multi-level splitting of finite element spaces. Numer. Math., **58**, 163-184, 1990.
[69] H. Yserentant, Old and new convergence proofs for multigrid methods. Acta Numerica **2**, 285-326, 1993.
[70] E. Zeidler, Nonlinear Functional Analysis and Its Applications. II/A: Linear Monotone

Operators. Springer, Berlin-Heidelberg-New York, 1990.
[71] L. Zhong, L. Chen, S. Shu, G. Wittum, and J. Xu, Quasi-optimal convergence of adaptive edge finite element methods for three dimensional indefinite time-harmonic Maxwell's equations. submitted, 2010.
[72] L. Zhong, L. Chen, and J. Xu, Convergence of adaptive edge finite element methods for H(curl)-elliptic problems. Numer. Lin. Algebra Appl. **17**, 415-432, 2009.